Broad Band Modelling of Electromagnetic Wave Coupling to Scatterers Inside a Metallic Cavity

J. v. Hagen, Student Member* W. Tabbara, ACES Member* D. Lecointe**

*Division Ondes, Laboratoire des Signaux et Systèmes/CNRS
**Service d'Electromagnétisme
*,**Supélec, Plateau de Moulon, F – 91192 Gif-sur-Yvette

Abstract

In this paper we present an approach based on the method of moments for the solution of an electromagnetic compatibility problem. We determine the results of the impact of an electromagnetic wave on metallic housings with small holes. By separating the interior and the exterior of the housing we are able to use the Green's functions of the cavity. The number of unknowns is therefore reduced compared to solutions using the free space Green's functions. Different sets of functions (either local or global) are used for the method of moments (MoM). Furthermore, we present a method to generate broad band data from only a few computations by using an "intelligent" interpolation procedure. Finally, we present an experimental setup and compare our computations with measurements.

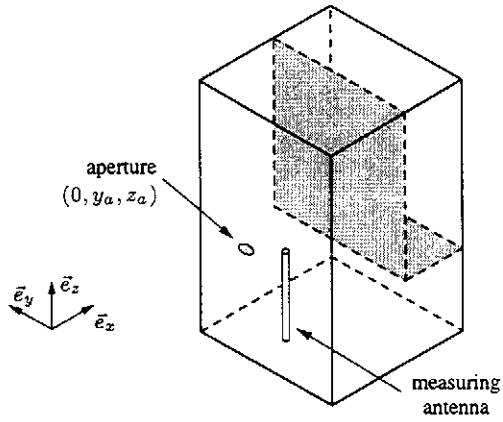

Figure 1: Typical cavity with monopole antenna and large plate

1 Introduction

Coupling of electromagnetic energy into cavities through one or more holes in its walls is one major problem in the domain of electromagnetic compatibility. This configuration is subject of several papers which concentrate on numerics or experiments. Taflove and others used the Finite-Difference Time-Domain approach, also coupled to the Method of Moments [1]. Others take a more overall look of the problem [2], while comparison between the Finite-Difference Time-Domain approach, the Method of Moments and experiments can be found in [3]. In the present paper, we will use the MoM to compute the currents in the cavity when excited by a plane wave. In doing so, we aim to understand more closely the phenomena of coupling and the physical aspects related to them. Our method is also applicable to other generic cavities as cylindrical ones with additional walls changing their shape so that the use of closed form Green's functions would not be possible.

A typical cavity is shown in fig. 1. Electrically, it is a non cuboidal cavity with an aperture in one wall. A non cuboidal cavity in this sense is a cavity not necessarily having rectangular walls. Conducting wires or plates are placed inside the cavity. A plane wave comes on the structure from the front, interacting with the objects in the interior of the cavity. In the case we will consider here, the object is a monopole antenna. In the experimental setup, this antenna is connected to a network analyser for measuring the received power and hence the current at the base.

The structure of this paper is as follows: first, we will describe the method used. We will focus especially on the reduction of the computational effort and the choice of appropriate basis and testing functions. In a second part, we present a method to create broad band data from only a few computations by means of an interpolation scheme. In a third part, we will compare results of computation and experimental measurements for some representative cases. A short conclusion is at the end.

2 Method

An incident field is created by a plane electromagnetic wave entering the cavity through the aperture. The equivalent dipole method [4] enables us to separate the interior from the exterior by metallizing the aperture and replacing it by two

dipoles, an electric and a magnetic one. The dipoles represent the two major characteristics of the hole, that is its size and shape, as well as the field strength: size and shape are translated by the dipole polarizabilities which are multiplied by the difference of the short circuit fields across the metallized aperture. Collin [4] and later de Meulenaere [5] found polarizabilities for various shapes based on considerations by Bethe. For various apertures the polarizabilities have the property of being independent of the actual aperture shape when normalised by a power of the aperture surface $A^{3/2}$.

In the following, we will consider an aperture with a normal along $\vec{e}_x$. Generally, the two major directions of the aperture (e.g., the major and minor axis for an elliptical aperture, or the two sides of a rectangular one) are directed in the $\vec{t}_1$ and the $\vec{t}_2$ direction normal to $\vec{e}_x$. The dipole moments are given by [5]:

$$\vec{P}_e = \varepsilon a_e E_{nsc} \vec{n} \quad \text{and} \quad \vec{P}_m = -2\bar{\bar{a}}_m \vec{H}_{sc} \tag{1}$$

with E_{nsc} the electric field normal to, and $\vec{H}_{sc}$ the magnetic field across the metallized aperture. a_e, $\bar{\bar{a}}_m$ are the scalar electric and the dyadic magnetic polarizabilities. For circular apertures with radius r they are given by:

$$a_e = \frac{2r^3}{3} \quad \text{and} \quad \bar{\bar{a}}_m = \frac{4r^3}{3}\left(\vec{t}_1\vec{t}_1 + \vec{t}_2\vec{t}_2\right) \tag{2}$$

The dipole approximation is valid for the fields at some distance of the aperture. The limit of validity is directly related to the aperture size [6]. Furthermore, the aperture should not be closer than its typical dimension (the aperture's diameter or largest dimension) to the cavity walls.

The aperture now being metallized, we use the closed form Green's functions of the rectangular cavity to express the total electric field inside the cavity as a function of the fields radiated by the dipoles and the induced current on the scatterers like the plates forming a corner in fig. 1. The Green's functions are triple trigonometric series. They can be found, e.g.,in [7] or [8], and are not given here for the sake of brevity.

As the Green's functions of the cavity already include the boundary conditions, we do not need to discretize the walls. Therefore the number of unknowns stays small, a typical number would be 500 for a $2\lambda \times \lambda \times \lambda$ cavity with a $\lambda \times \lambda \times \lambda/2$ object inside and a discretization rate of $\lambda/10$.

Finally, we include the boundary conditions for the electric field on the metallic objects inside the cavity which force the tangential electric field to zero:

$$\vec{n} \times \vec{E}(r) = \vec{n} \times \left(\vec{E}_i(r) + \vec{E}_s(r)\right) = 0$$
$$\text{for all } r \text{ on a perfect conductor} \tag{3}$$

with $\vec{n}$ normal vector on surface, $\vec{E}_i$ incident field and $\vec{E}_s$ scattered field due to the currents induced on the metallic objects. This equation becomes by using the Green's functions

$$\begin{aligned}\vec{n} \times \vec{E} &= \vec{n} \times \left(\vec{E}_i + \vec{E}_s\right) \\ &= \vec{n} \times \left(\int_{P_e} \bar{\bar{G}}_e \vec{P}_e \, dP_e \right. \\ &\left. + j\omega\mu \int_{P_m} \bar{\bar{g}}_e \vec{P}_m \, dP_m \right) \\ &+ \vec{n} \times \frac{j}{\omega\varepsilon}\left(\nabla^2 + k^2\right) \int_J \bar{\bar{G}}_A \vec{J} dJ = 0 \end{aligned} \tag{4}$$

$\bar{\bar{G}}_A$, $\bar{\bar{G}}_e$ and $\bar{\bar{g}}_e$ are the Green's functions of the vector potential, of electric dipoles and of magnetic dipoles respectively. The reaction of the scatterers as well as of the cavity can be included in the formulation. In this case, three additional unknowns which are the difference of the normal electric field (one unknown) and the tangential magnetic field (two unknowns) between the field inside and outside of the cavity across the aperture appear. If the cavity would be mounted behind an infinite screen, these unknowns are easily evaluated as the incident fields. In the general case of a cavity in free-space or some other environment, the short circuit fields can be determined numerically and the included into the solution. We do not include this here for the sake of clarity. In fact, the influence of the reaction was evaluated as neglectable in comparison with measurements in [9]. Neglecting the reaction of scatterers and cavity sets E_{nsc} and $\vec{H}_{sc}$ in eqn. (1) to the values of the incident field of the oncoming wave. We solve the integral equation eqn. (4) by a method of moments [10]: first, we expand the unknown surface currents J in an appropriate set of basis functions f_i, then project the equation on a set of testing functions w_i. This finally leads to a linear system of equations

$$\mathbf{Z}I = V \tag{5}$$

The so-called impedance matrix $\mathbf{Z}$ is composed of the integrals in (4), the vector I contains the unknown projection of the surface currents J on each basis functions f_i, and V contains the incident field.

The choice of the functions f_i and w_i involved must take into account the following considerations:

- the sum of the continuous differentiability of the basis and testing functions should be greater than 1 [11]. Therefore, using the piecewise continuous function (or pulse function) as both basis and testing functions is not valid.
- ease of implementation. Several functions offer the possibility to carry out analytically the integration of the Green's function with the expansion functions and the integration due to the Method of Moments. We therefore will focus on this kind of functions.

- nature of functions. In the following, we will point out that the use of domain functions is preferable to strictly local functions.
- number of functions involved and therefore size of matrix.

In the following, we will touch upon further reducing the computational effort and choosing of basis and testing functions.

2.1 Efficient summation of the Green's functions

Several papers are available for the acceleration of the computation of Green's functions. They yield reasonable results for periodic free space functions [12]. In our case, the application of these purely mathematic algorithms appear to be less efficient than an 'intelligent' summation of the series. We will explain this approach which is based on the works of Seidel [7].

The Green's functions are given as a triple series of trigonometric functions. We can always sum up one series for one coordinate direction analytically (see [4] for a list of known expressions), so that the triple series is reduced to a double one in the two remaining directions. The analytical expression includes an exponential function which renders the convergence very fast. The series (supposing that we reduce the series in z) depends now on the other two indexes combined by a function as

$$f(l_y, l_z) \exp\left(-\pi \sqrt{\frac{{l_x}^2}{A} + \frac{{l_y}^2}{B}}\,|z - z'|\right) = f(l_y, l_z) \exp\left(-\pi\, k_c\, |z - z'|\right) \qquad (6)$$

where l_x and l_y are the indexes in x and y direction and, in fact, the indexes for the eigenmodes of the empty cavity. A and B are the dimension of the cavity in x and y. The new sum will now rapidly converge when ordered such that k_c (depending now on a new summation index q) $k_c(q)$ grows steadily. One has now effectively reduced the double indexed series to a normal one with the new summation index q. The choice of the ordering scheme is outlined in fig. 2 for the first ten terms and for a cavity with different size in $x = 0.3$ m and $y = 0.5$ m. Each solid lines relates to one value of q and several pairs of (l_x, l_y). For a given q there are several l_x and l_y with a k_c of almost the same value. Proceeding to a next q will give a larger k_c, and therefore a much smaller term in the series. One easily sees that for a given value of q there are approximately q^2 terms to evaluate.

In eqn. (6) we do not have exponential convergence, when the observation point has the same z–coordinate as the source point ($z = z'$). In this case, a quite important number of terms is necessary to insure convergence (see further down).

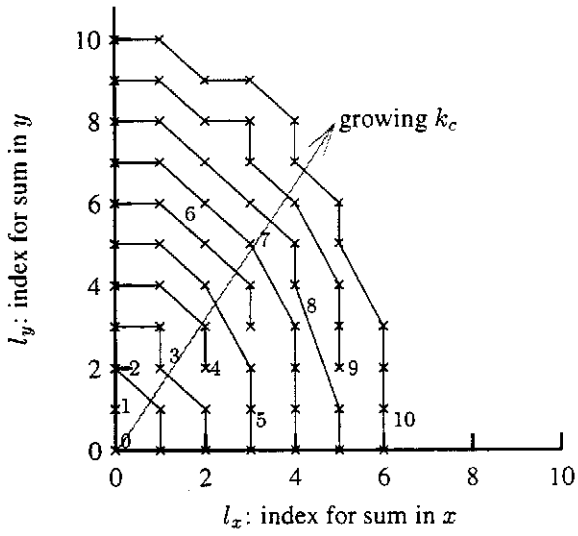

Figure 2: Ordering scheme for efficient computation. The numbers in the graph are index q for final sum

2.2 Possible basis and testing functions

A fast convergence of the method to the right value is only possible if the basis function set is closely approximating the physical reality. The choice of the basis and the testing functions is therefore a crucial step during the application of the Method of Moments. Two schemes for the discretization are possible: a strictly local one where the support of the functions is a sub-domain of the support of the unknown physical solution. Possible are rectangular and triangular supports. Another possibility are global domain functions whose support coincides at least in one coordinate direction with the support.

A wide range of functions was used for scattering computations in thin wire and 3D geometries. In this paper, we will concentrate on the following generic functions (let $\hat{x} = \frac{x - x_0}{\Delta_x}$ be the normalised and centred x-coordinate):

- point matching (Dirac pulse) $D(x) = \delta(x - x_0)$
- piecewise constant or pulse $CT(x) = 1$ for $|\hat{x}| < 0.5$, 0 elsewhere
- piecewise linear or triangle $LI(x) = 1 - |\hat{x}|$ for $|\hat{x}| < 1$, 0 elsewhere
- piecewise sinusoidal $SI(x) = \frac{\sin k\Delta_x(1-|\hat{x}|)}{\sin k\Delta_x}$ for $|\hat{x}| < 1$, 0 elsewhere
- global-domain functions with sine or cosine behaviour in direction of the current and constant normal to it with corresponding edge–conditions

For fine discretizations the piecewise linear and the piecewise sinusoidal functions are equivalent, as also a Taylor series of the sine-function would prove. Fig. 3 shows the graph of some functions applied for surface currents on three-dimensional plane conductors. Here, the one–dimensional functions for one coordinate are multiplied by the same (or another) one–dimensional function so that the resulting function is still separable. In this way, the integrations can be carried out for the two coordinate directions independently. When applied to our case of plane conductors in cavities, they offer the advantage of an analytic integration of Green's function over the basis/testing functions. Furthermore, the piecewise linear and sinusoidal functions lead to expressions that decrease rapidly with the summation index so that even for observation and source points in the same plane, the series in eqn. (4) converge.

A special treatment is necessary for functions at the edges of conductors. In the case of triangular functions parallel to an edge one has to use half-triangles at the edges to account for the right place of the match point. The incorporation of special edge elements as normally used in spectral domain methods is possible [13], but is of only minor importance in our case. We therefore did not include them in the present paper.

In the case of a current normal to an edge, two cases must be distinguished. The first is an isolated plate, where the current normal to the edge goes to zero. The corresponding function is therefore constant zero to produce the right boundary condition. The second possibility is when two plates are connected to each other. In this case, the current has to be continuous over the edge which is included by two half-width functions with the same amplitude. A plate connected to a cavity wall falls also under this category, no special treatment, however, is needed. The continuity of the current with the image of the plate is provided by the Green's functions. provided

Based on the reflections of Aksun [11], we will consider the following combinations of basis and testing functions (first is basis, second is testing function, abbreviations in parenthesis): pulse – triangle (CT–LI), pulse – sinusoidal (CT– SI), triangle – triangle (LI–LI), sinusoidal – sinusoidal (SI–SI). The latter two combinations are Galerkin solutions and offer therefore the possibility to compute only half of the now symmetric impedance matrix.

Another possible choice for basis/testing functions are global domain functions. To use these functions we 'cut' the plane conductor into several strips. The functions used are now the products of sine or cosine functions in the direction of the current and a local function (usually the piecewise constant function) in the direction normal to it. We use the name *global* functions despite the fact that the functions are not global, i.e. defined on the whole support, in the direction normal to the direction of the current. The condition for the choice for sine or cosine function is the condition for the current at the ends of the strips:

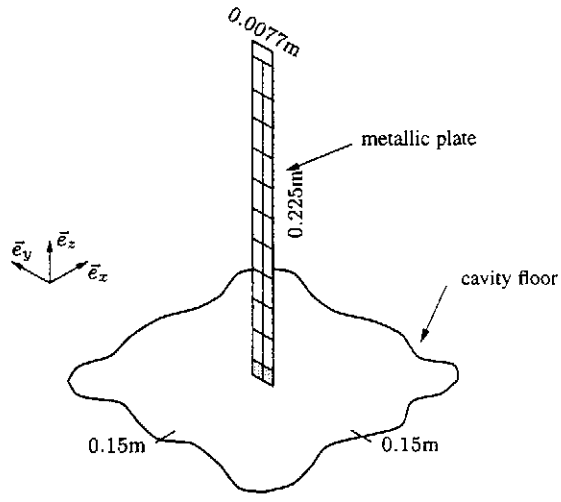

Figure 5: Discretization of test case

- $\sin\left(\frac{m\pi}{2}\frac{x-x_{min}}{x_{max}-x_{min}}\right)$ for isolated conductors (the current goes to zeros at both ends)
- $\cos\left(\frac{2m+1}{2}\pi\frac{x-x_{min}}{x_{max}-x_{min}}\right)$ for conductors attached to others at $x = x_{min}$ (the current goes to zero at $x = x_{max}$)
- $\cos\left(\frac{2m+1}{2}\pi\frac{x_{max}-x}{x_{max}-x_{min}}\right)$ for conductors attached to others at $x = x_{max}$ (the current has a zero at $x = x_{min}$. For $m = 0, 1, 2$ shown in fig. 4).
- $\cos\left(m\pi\frac{x-x_{min}}{x_{max}-x_{min}}\right)$ for conductors attached to others at both ends (no zeros at x_{min} or $x = x_{max}$).

These global functions lead to smaller matrix systems compared to the local basis functions. Also interesting is the fact that an impedance matrix for a discretization order $n+1$ is simply constructed by the matrix of order n with one additional row $n+1$ and one additional column $n+1$ for the new functions f_{n+1} and w_{n+1}:

$$\mathbf{Z}_{n+1} = \begin{pmatrix} Z^{1..n,1..n} & Z^{1..n,n+1} \\ Z^{n+1,1..n} & Z^{n+1,n+1} \end{pmatrix} \tag{7}$$

One can calculate a matrix $\mathbf{Z}_n$ for a given discretization, calculate the currents on the metallic objects, then increase the order of the discretization and calculate just one more matrix row $Z^{n+1,1..n+1}$ and column $Z^{1..n,n+1}$ while still preserving the other elements. We then can recalculate the currents and stop this iterative process when convergence is achieved.

As a test case for the different functions we calculate the current on a rectangular plate of width 0.0077 m in $\vec{e}_y$ and length 0.225 m in $\vec{e}_z$ as shown in fig. 5. It is connected to the cavity floor at the point with the coordinates

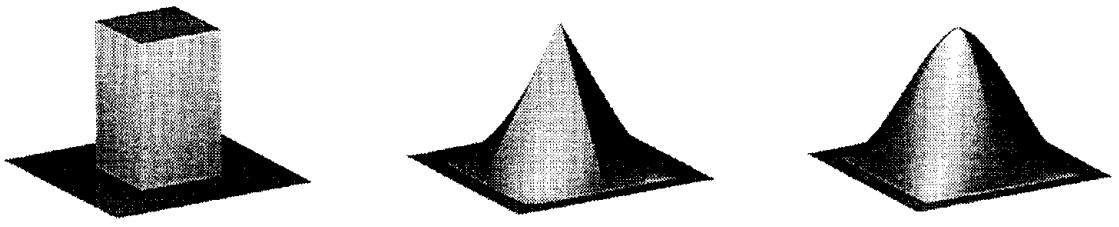

(a) Pulse (b) Triangle (c) Piecewise sinus.

Figure 3: Possible local functions: 3(a) pulse, 3(b) piecewise linear (triangle), 3(c) piecewise sinusoidal.

(a) first (b) second (c) third

Figure 4: First three global domain functions

$(0.15, 0, 0.15)$ m. The cavity has the dimensions 0.297 m, 0.297 m, 0.498 m. Frequency is 800 MHz with incidence in $\vec{e}_x$ direction, the circular aperture with radius $r = 0.02$ m is centred on the wall $x = 0$. The current I at the base of this plate (i.e. the integral of the current densities over the two cells at the base which are located at $y = 0.14465$ m and $y = 0.15235$ m, grey in fig. 5) is shown in fig. 6 as a function of discretization order n. We see that all three curves converge to nearly the same value (relative error less than 2 %), but that the matrix size needed for stable values is much smaller for global domain functions than for local ones (9 vs. 12). We get quite good results with only 4 functions with an error of 0.1% in the evaluation of the current. As all integrations are carried out analytically, the computation time for one matrix element at a given discretization order is the same for all functions, which is not the case if one uses the free space Green's functions.

In fig. 7 we plot the maximum value of l_y and l_z (as the series is reduced in x, the indexes are in this case l_y and l_z) needed for obtaining a convergence to $\pm 0.15\%$ (shown as dashed lines) for the current on the same plate. Discretization on the plate was 2 cells in $\vec{e}_y$ and 20 in $\vec{e}_z$. For the global functions only 8 functions were used. All combinations of functions yield the same current at the base. The maximum for l_y and l_z is also the same: 150 to 200 (this corresponds

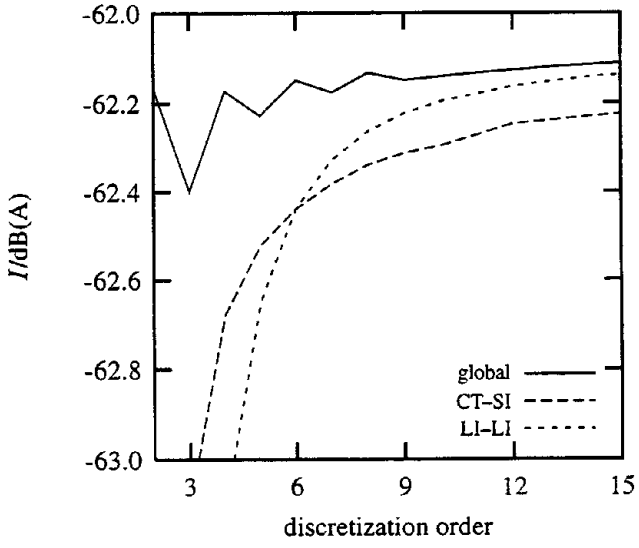

Figure 6: Convergence by discretization

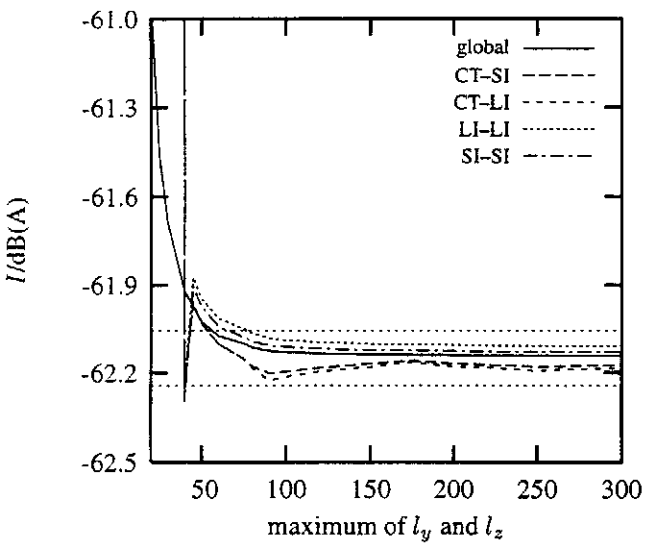

Figure 7: Convergence by number of modes

to about 71000 single terms to evaluate).

With these results in mind, we can choose our basis and testing functions with the ease of implementation in mind. This is especially necessary if one considers currents on plates connected to each other. We use the piecewise continuous–piecewise sinusoidal combination. This set has the advantage that the mentioned reduction of the three–dimensional series to the two–dimensional one yields expressions which enhance convergence. For smaller matrices and therefore faster computations we recommend nevertheless the use of global functions. As a matter of fact, for the same structure and a difference of the currents of smaller than 0.1 % to the final solution we needed 14 functions for the CT–SI case, 12 functions for the LI–LI case and only 9 functions for the global case.

This procedure is also valid for objects behind metallic screens. Simulations for this case not shown here resulted in currents on metallic objects and the resulting fields behind metallic screens in the order of numeric noise.

A short comment on the computation times. Typical simulations were run on SUN Sparc 20 or Ultra 1/2 computers, with RAM ranging from 64 to 256 MB. Due to our method, only small memories are needed, in fact 64 MB are sufficient to run any geometry we considered. Typical execution times per frequency are several seconds for simple cases (10 s for the case in fig. 5) to several minutes for more complicated cases.

3 Broad band data

Though the computational cost is lower when using the Green's functions of the cavity than by using the free space functions, a computation for several frequencies can become quite time consuming. In this section we describe a method to generate broad band data from just a few computations. This method is based on a similar one proposed in [14] for free space.

For computations at several frequencies the impedance matrix would have to be built for several frequency points. On the other hand the terms in the impedance matrix show only a slow evolution with frequency except at the resonances of the empty cavity. As a matter of fact the Green's functions have singularities at the resonance frequencies. A classic interpolation using polynomials would not accurately model the behaviour of the individual matrix terms. However, an interpolation with a rational function of order $\mu + \nu + 1 = \rho + 1$ in the form

$$R^{\rho} = \frac{p_0 + p_1\, x + \cdots + p_\mu\, x^\mu}{q_0 + q_1\, x + \cdots + q_\nu\, x^\nu} \tag{8}$$

with q_0 arbitrary and $\mu \leq \nu$ would well approximate these singularities. $\rho + 1$ will be the number of knots or matching points of the scheme. An interpolation scheme for rational functions with these characteristics is known [15, 16].

As the poles of the Green's functions are the resonances of the empty cavity, their location on the frequency–axis is known and can easily be computed. It is now possible to subdivide the whole wanted frequency band into smaller sub-bands, limited by two resonance frequencies $[f_i, f_{i+1}]$. For the location of the knots of the interpolation scheme in the corresponding frequency sub-band we use two different schemes: the first one is a uniform distribution of the knots. In this case the knots are given by

$$f^k = f_i + \frac{f_{i+1} - f_i}{\rho}\, k \qquad \text{for} \quad k = 0 \ldots \rho \tag{9}$$

A widely used interpolation scheme [17], is the Tchebycheff scheme, leading to

$$f^k = \frac{f_i + f_{i+1}}{2} + \frac{f_i - f_{i+1}}{2} \cos\left(\frac{2k+1}{2n+2}\,\pi\right) \tag{10}$$

This choice yields better results for the interpolated values at the ends of the sub-bands and is therefore better suited.

The number of knots necessary to get an appropriate interpolation depends on the density of resonances in the vicinity of the sub-band. If the influence of one resonance is still strong in the sub-band, we need 5 knots in one band. For largely spaced resonances there are only 4 knots needed. This can be seen in fig. 9 where we traced for a cavity described further down the measurement data, the simulation and the interpolated simulation. For the sub-bands between 700 MHz and 790 MHz with 3 closely spaced resonances at 704.750 MHz, 765.554 MHz and 778.422 MHz, we need 5 knots for a reasonable interpolation. For the other sub-bands (e.g. for the two first bands between 0 and 300 MHz

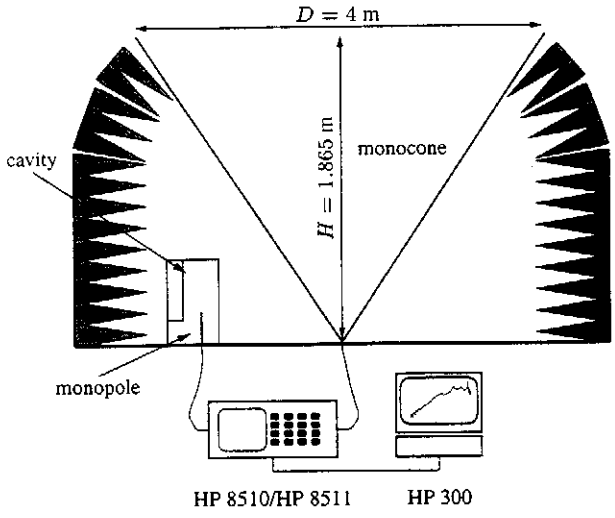

Figure 8: Experimental setup with monoconic antenna, monopole and network analyser

and 300 MHz and 600 MHz) below and above, the interpolation scheme is almost perfect with this number of knots. For the present calculation we cut the whole band into 10 sub-bands and interpolated the matrices in a frequency step of 5 MHz. The time to build the 50 matrices was about 38 hours, the interpolation time to create the other 164 matrices was 18 minutes. If all 214 matrices were calculated a total time of 160 hours would have been necessary.

4 Simulations and experiments

For comparison purposes the above mentioned cavity was placed in an semi–anechoic chamber without absorbers on the floor. The incident plane wave was created by a monoconic antenna, the response of the system measured by a monopole–antenna based on the metallic floor of the chamber. The monoconic antenna (with its image) is able to provide a plane wave over a wide frequency band. The low–SWR monoconic antenna was driven by a HP 8510 network analyser which also measured the response of the monopole. First, we determined the field present in the chamber without any object. Thus we get the incident field. For the subsequent measurements we read the transfer coefficient S_{21} of the system monoconic-antenna–cavity–monopole and related it to the previously measured incident field. We therefore trace the received power for a normalised incident plane wave of $E = 1\frac{\mathrm{V}}{\mathrm{m}}$. The experimental setup is sketched in fig. 8.

The monopole for measurements was modelled by a thin strip using the expression for equivalent radii given by Einarsson [18]. The equivalent radius r of a wire for a plate of width d is

$$r = \frac{d}{4} \tag{11}$$

Several configurations were measured to test our computations. In a previous paper [19] we presented data for single monopoles in the cavity, the results presented here concern the case where several metallic objects are placed inside a cavity. The objects can be in a conducting or isolated contact with one or several cavity walls. The shape of the cavity can be changed by including large objects in contact with the walls. When using the appropriate plates like shown in fig. 1 one can easily model the cavity with reentrant corner of fig. 9. This was acheived by placing plates into the cavity and connecting them using conducting tape.

The geometrical data are as follows: cavity size 300 mm, 300 mm, 500 mm, aperture diameter 20 mm centred on the $x = 0$ mm wall of the cavity. The monopole antenna has a radius of 1 mm and a length of 300 mm. It stands on the base of the cavity at 110 mm from the aperture, also centred in y. The reentrant corner is the upper back corner of the cavity. It covers the hole section in y, and from $z = 100$ mm to the top of the cavity. The depth is 110 mm. A comparison between the simulated and measured data is shown in fig. 9. The agreement is good. At very low frequencies the expected high–pass behaviour is observed with a +40 dB/decade rise with frequency [9]. The $\lambda/4$ resonance of the monopole at 600 MHz is mixed with a first resonance of the cavity with reentrant corner geometry. For higher frequencies we can not yet identify the different resonances. Some comments should be made upon some details of the curve. The simulations suppose perfectly conducting cavity walls, the resonnances would have a very high quality factor. The experimental cavity has not this high quality factor, the differences at the resonnances are due to this fact. Furthermore, the experimental data include some artefacts due to the fact that the corner was made by conducting tape and not by soldering.

5 Conclusion

We have presented a Method of Moment solution for the coupling of electromagnetic energy into cavities. The method is based on the electric field integral equation. It separates interior from the exterior by the equivalent dipole method. By placing metallic plates into the cavity, it is possible to easily change the shape of the latter without changing the scheme. The Green's functions of the rectangular cavity are used, so that only the scatterers are discretized, the number of unknowns is thus kept small. In the Method of Moments we have studied several sets of basis and testing functions with support either over the whole scatterer or only parts of it. They all yield the same result for fine discretizations. All functions have, however, particularities so

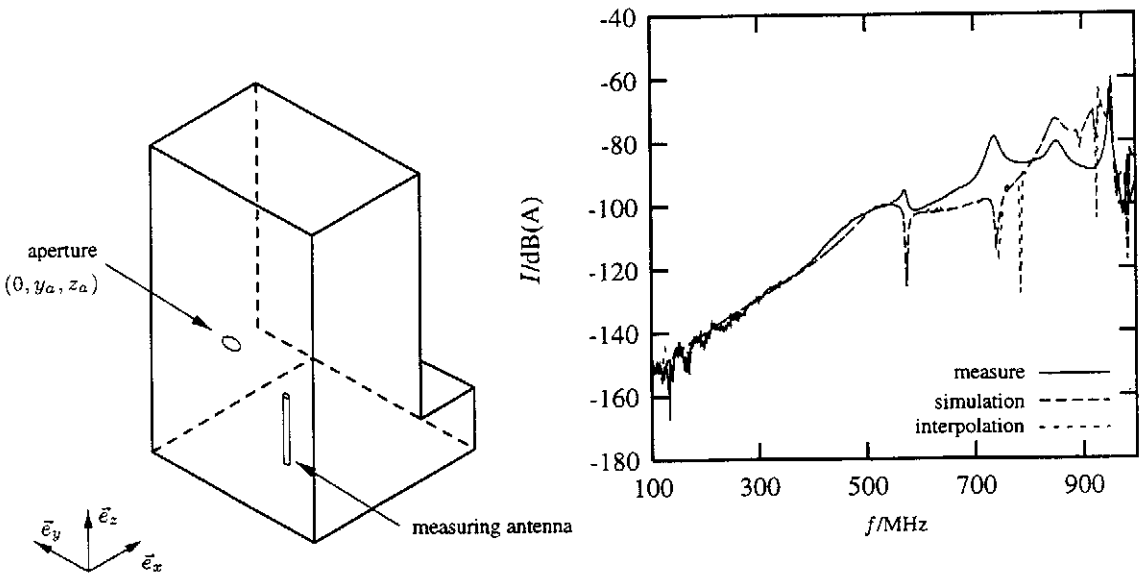

(a) Cavity with reentrant corner

(b) Measurement and simulation

Figure 9: Comparison measurement/simulation

that we tend to use specific sets in one case or another.

Comparisons of computations and simulations attest the efficiency of the method proposed, simulations leading to current values close to the measured ones.

Acknowledgements

The authors would like to express their thanks to J.-L. Lassere and J.-L. Lavergne as well as to the Centre d'Etudes de Gramat for making the measurements possible.

References

[1] A. Taflove and K. Umashankar, "The Finite-Difference Time-Domain (FDTD) Method for electromagnetic scattering and interaction problems," *J. Electromag. Waves Appl.*, vol. 1, no. 3, pp. 243–267, 1987.

[2] D. A. Hill, M. T. Ma, A. R. Ondrejka, B. F. Riddle, M. L. Crawfors, and R. T. Johnk, "Aperture excitation of electrically large, lossy cavities," *IEEE T-EMC*, vol. 36, no. 3, pp. 169–177, Aug. 1994.

[3] B. Chevalier, B. Pecqueux, J. Lasserre, and D. Lecointe, "Détermination du couplage sur un fil placé à l'interieur d'une cavité métallique," *CEM 1994, Toulouse*, 1994.

[4] R. E. Collin, *Field Theory of Guided Waves*. New York, Toronto, London: McGraw-Hill, 1960.

[5] F. de Meulenaere and J. van Bladel, "Polarizability of some small apertures," *IEEE Trans. Ant. Prop.*, vol. 25, no. 2, pp. 198–205, March 1977.

[6] Y. Rahmat-Samii and R. Mittra, "Electromagnetic coupling through small apertures in a conducting screen," *IEEE Trans. Ant. Prop.*, vol. 25, no. 2, pp. 180–187, March 1977.

[7] D. B. Seidel, "Aperture excitation of a wire in a cavity," PhD-thesis, University of Arizona, Arizona, 1977.

[8] C.-T. Tai, *Dyadic Green Functions in Electromagnetic Theory*. Piscatawy, NY: IEEE Press, 1994.

[9] D. Lecointe, *Détermination du couplage d'une onde électromagnétique avec un câble situé dans une cavité métallique*. PhD thesis, University of Paris VI, France, 1995.

[10] R. Harrington, "The method of moments in electromagnetics," *J. Electromag. Waves Appl.*, vol. 1, no. 3, pp. 181–200, March 1987.

[11] M. Aksun and R. Mittra, "Choices of expansion and testing functions for the Method of Moments applied to a class of electromagnetic problems," *IEEE Trans. Micro. Theo. Tech.*, vol. 41, no. 3, pp. 503–509, March 1993.

[12] S. Singh and R. Singh, "On the use of Levin's T-transform in accelerating the summation of series representing the free-space periodic Green's functions,"

IEEE Trans. Micro. Theo. Tech., vol. 41, no. 5, pp. 884–886, May 1993.

[13] D. Wilton and S. Govind, "Incorporation of edge conditions in moment method solutions," *IEEE Trans. Ant. Prop.*, vol. 25, no. 6, pp. 845–850, Nov. 1977.

[14] E. H. Newman, "Generation of wide-band data from the method of moments by interpolating the impedance matrix," *IEEE Trans. Ant. Prop.*, vol. 36, no. 12, pp. 1820–1824, Dec. 1988.

[15] J. Stoer, "Über zwei Algorithmen zur Interpolation mit rationalen Funktionen," *Numerische Mathematik*, vol. 3, pp. 285–304, 1961.

[16] W. H. Press, S. A. Teukolsky, W. T. Vetterling, and B. P. Flannery, *Numerical Recipes in C.* Cambridge, New York and Melbourne: Cambridge University Press, 1992.

[17] R. Bulirsch and H. Rutishauser, "Interpolation und genäherte Quadratur," in *Mathematische Hilfsmittel des Ingenieurs* (R. Sauer and I. Szabó, eds.), no. H in Teil III, Berlin, Heidelberg: Springer–Verlag, 1968.

[18] O. Einarsson, "The Wire," in *Electromagnetic and Acoustic Scattering by Simple Shapes* (J. Bowman, T. Senior, and P. Uslenghi, eds.), Amsterdam: North-Holland Publishing Company, 1969.

[19] D. Lecointe, W. Tabbara, and J. Lasserre, "Aperture coupling of electromagnetic energy to a wire inside a rectangular metallic cavity," *IEEE Ant. Prop. Soc. Int. Symp.*, vol. 3, pp. 1571–1574, July 1992.